ORIGINAL ARTICLE

Synthesis and characterization of an innovative sodium alginate/ flaxseed gum green hydrogel for forward osmosis desalination

Menatalla Ashraf Saad[1] · Eman Radi Sadik[4] · Basma Mohamed Eldakiky[4] · Zhen He[5] · Elsayed Zakaria Elashtoukhy[1] · Randa Eslah Khalifa[2] · Taghreed Mohamed Mohamed Zewail[1] · Hanan Moustafa[3]

Abstract

Recently, fresh water resources have been limited globally. Thus, desalination has been the most recommended solution to overcome this issue. Forward osmosis (FO) is an affordable and developing desalination technique. In this current study, a cutting-edge green hydrogel was prepared from a polymer blend of flaxseed gum (FG) and sodium alginate using epichlorohydrin (ECH) as a crosslinker and polyethylene glycol (PEG) as a semi-interpenetrating network polymer. The impact of PEG incorporation on the hydrogel's response was investigated, and the influence of different mass contents of FG and ECH on the swelling measurements of the hydrogel was studied to optimize the composition of the hydrogel. The optimum hydrogel was characterized by Fourier transform infrared spectroscopy, scanning electron microscopy, and X-ray diffraction and the compressive strength test. Furthermore, the behavior of the present hydrogel was examined as a draw agent in a batch FO unit. The water flux and the reverse solute flux were measured at various values of average hydrogel particle size and feed solution (FS) temperature and concentration. The optimal hydrogel of 0.3 PEG/polymer blend mass ratio, 12% FG, and 0.95 ECH/polymer blend mass ratio exhibits a swelling ratio (%) of 1800 after an hour and an equilibrium swelling ratio (ESR) (%) of 5300. The results of the FO experiments revealed that raising FS temperature and reducing FS concentration and average hydrogel particle size enhance water flux.

Keywords Sodium alginate · Flaxseed gum · Green hydrogel · Draw agent · Forward osmosis · Desalination

Introduction

Water is the most precious resource on the planet for survival (Jain et al. 2022a). The exponential growth of human populations is considered a serious challenge that faces our universe nowadays (Zhao et al. 2012). This can negatively reflect on global water and energy consumption. Furthermore, contamination of current fresh water resources (such as freshwater lakes and groundwater) by home and industrial wastes exacerbates fresh water scarcity (Wen et al. 2023). Recent international reports revealed that mostly one-third of the population in our universe will be suffering from water scarcity by 2025, and from 2007 to 2035, it is expected that global energy consumption will rise by 49% (USAID 2009; Zhao et al. 2012).

However, water covers more than two-thirds of the surface of the Earth; the majority of this water is saltwater, and freshwater covers only 3% of the water that exists on this planet. From this perspective, desalination is the best solution for freshwater production (Baker et al. 2016;

✉ Menatalla Ashraf Saad
  mennat.ashraf@alexu.edu.eg

1 Chemical Engineering Department, Faculty of Engineering, Alexandria University, Alexandria 21544, Egypt

2 Polymer Materials Department, Advanced Technologies and New Materials Research Institute (ATNMRI), City of Scientific Research and Technological Applications (SRTA City), P.O. Box: 21934, New Borg El-Arab City, Alexandria, Egypt

3 Biotechnology Department, Institute of Graduate Studies and Research, Alexandria University, Alexandria 21526, Egypt

4 Chemical Engineering Department, Borg Al Arab Higher Institute of Engineering and Technology, Alexandria 21933, Egypt

5 Department of Energy, Environmental and Chemical Engineering, Washington University in St. Louis, St. Louis, MO 63130, USA

Ohtani 2021). Typically, saline water can be desalinated by two distinct technologies, namely thermal and membrane approaches (Younos and Tulou 2005; Ankoliya et al. 2019). Membrane-based desalination processes, including reverse osmosis (RO), are more energy-efficient than thermal-based technologies. Lately, forward osmosis (FO) has established as a novel desalination approach that saves more energy than other desalination technologies (Altaee et al. 2014; Jain et al. 2022b). FO uses the natural osmotic pressure to transport freshwater from the FS side to the drawing side through a semipermeable membrane because of the osmotic pressure difference (Suwaileh et al. 2020). FO is distinguished over other desalination techniques by its low-fouling tendency and its limited energy requirements. Nevertheless, the selection of the appropriate drawing solute that provides enhanced driving force and the ability to be regenerated is the most critical challenge facing the FO desalination process (Zhao et al. 2012).

The most common organic draw agents are oligomers and hydrogels, while NaCl and ammonium carbonate solutions are widely applied as DS in FO desalination. Presently, the demand for the usage of hydrogels as drawing agents in FO desalination has grown owing to their low level of toxicity, low reverse solute flux, and enhanced water absorption capacity (Suwaileh et al. 2020). Hydrogels can be characterized as 3D networks that are manufactured from polymer materials and have the ability to capture a definite quantity of water within their structures (Chatterjee and Hui 2018). Table 1 represents multiple instances of hydrogels used as draw agents in the FO process, the applied feed solutions, and the achieved water fluxes.

Green hydrogel is a new trend in hydrogel manufacture that is made of bio-renewable natural polymeric materials that are distinguished by their cheapness, easy accessibility, biocompatibility, and eco-friendliness. It is widely used in medical and agricultural applications (Mohammadinejad et al. 2019, Allamraju 2021). The expression of semi-interpenetrating hydrogels can be used when there is an existing crosslinked network penetrated with another linear polymer without any chemical reaction. This design is used in various applications because of its high swelling rate and desirable mechanical characteristics (Matricardi et al. 2013).

Sodium alginate (SA) is a natural marine polymer that is extracted from brown algae (Merakchi 2019). It is made up of residues of 1,4-linked-D-mannuronic acid (M) and L-guluronic acid (G). Typically, SA is distinguished by its hydrophilicity and gelation features, so it is widely recommended in various applications such as tissue engineering or water treatment (Esposito et al. 2020). FG, which can also be called mucilage, is the soluble dietary fiber that exists in the outermost layer (hull) of flaxseed (Liu et al. 2018; Hu et al. 2020). It represents about 8% of the total seed mass and can be easily extracted by aqueous extraction (Liu et al. 2018). FG contains 80% of neutral and acidic polysaccharides and 9% of protein (Łopusiewicz et al. 2022). PEG is a synthetic polymer that has been extensively studied and is FDA-approved for use in biotechnology, medication delivery, tissue engineering, and water treatment. PEG has favorable qualities such as bio-inertness, hydrophilicity, superior mechanical characteristics, and adaptability (Zhu 2010; Chan et al. 2012; Ju et al. 2009). Epichlorohydrin was selected as a crosslinker because, in a basic medium, it behaves as a bifunctional molecule toward hydroxyl and/or amino group crosslinking (Bo 1992; Buhus et al. 2009).

The major goal of this study is to combine the eco-friendly characteristics of SA and FG green constituents (Khansari et al. 2017) and the high water absorbency and excellent mechanical properties of PEG (Zhu 2010) to form an innovative semi-interpenetrating SA/FG/PEG hydrogel. Furthermore, the synthesized hydrogel was applied as a draw agent in FO desalination. The impact of the percentage of the extracted FG in the polymer blend and the mass ratios of both PEG and ECH to the total polymer blend of SA and FG on the SR measurements was studied to optimize the composition of the hydrogel. The water flux and the reversed solute flux of the optimum SA/FG/PEG hydrogel were evaluated

Table 1 List of the most recent sorts of hydrogels applied as draw agents in FO desalination process

Type of the hydrogel	FS	J_W (LMH)	Reference
(2-acrylamido-2-methyl-l-propanesulfonic acid -co- acrylamide)/ polyacrylic acid electroresponsive hydrogel	2 g/L NaCl	2.2 (initial)	Xu et al. (2022b)
Poly (vinyl alcohol—diallyldimethylammonium chloride) hydrogel	5000 ppm NaCl	0.87 (average 6 h)	Bardhan et al. (2022)
(Isopropylacrylamide/sewage sludge ash) thermoresponsive hydrogel	2000 ppm NaCl	2.22(average 24 h)	Pan et al. (2022)
Dual carbon dioxide and thermoresponsive poly (N,N-dimethylallylamine) hydrogel	1.75% NaCl	44 (initial)	Ellis et al. (2021)
(Isopropylacrylamide/polyglutamic acid/polyethylene glycol) thermoresponsive hydrogel	Deionized water	1.99 (initial 0.5 h)	Zhang et al. (2020)
	0.05wt% NaCl	1.65 (initial 0.5 h)	
	0.1wt NaCl	1.31 (initial 0.5 h)	
	0.2wt% NaCl	1.08 (initial 0.5 h)	

in a batch FO unit under the influence of various parameters (e.g., average hydrogel particle size and FS temperature and concentration.

Materials and method

Materials

The utilized chemical materials, their purity, and their suppliers are defined in Table 2. All of these materials were used as they were supplied, with no further purification. Flaxseed was purchased from Al-Khaga Market (UAE). The National Research Center (Cairo, Egypt) provided the cellulose triacetate (CTA) membrane. The membrane's specifications are listed in Table 3. Samples of real brackish water were obtained from two distinct wells in Alamein City, Egypt. The membrane's specifications are listed in Table 3.

Flaxseed gum extraction

A certain amount of flaxseed was mixed with distilled water with a mass ratio of 1:10. Then, the mixture was heated until forming white foam at the surface. Then, the suspension was filtered through a stainless-steel drainer to separate the FG from the residue. These steps are quoted from the hot water extraction method (Hu et al. 2020).

Preparation of the hydrogel

A defined quantity of sodium alginate was dissolved in an 8% sodium hydroxide solution, and a defined quantity of PEG was also dissolved in distilled water. The SA and FG solutions were mechanically mixed for an hour to create a homogeneous solution. After that, the PEG solution was added to the mixture and mechanically stirred for 15 min. The total polymer (SA and extracted gum) concentration should be 6.8%. ECH was added dropwise to the blend, and the stirring continued mechanically to create a homogeneous paste. This paste was kept at 75 °C for 4.5 h. Then, distilled water that heated at 60 °C was used to wash the cured paste to get rid of all unreacted materials. Acetone was also used to eliminate any traces of ECH by the immersion of the paste in it for 10 min. Finally, the clean hydrogel was preserved at

Table 3 Specifications of CTA membrane

Material	Cellulose triacetate membrane
Hydrophilicity	Hydrophilic material
Color	White
Average pore diameter	1.21 nm
Porosity	36%
Tensile strength	33.5 MPa
Elongation	43.8%

50 °C for drying. Figure 1 represents all possible crosslinking reactions between SA and FG using ECH. The completely dried hydrogel was grinded and sieved into distinct average particle sizes starting from 112.5 to 462.5 μm. The impact of PEG/total polymer blend (0, 0.06, and 0.3) mass ratios, soluble extracted FG/total polymer blend (0, 12, and 100) mass percentages, and ECH/total polymer blend (0.95, 1.12, and 1.3) mass ratios on the SR of the hydrogel were studied.

Characterization of the hydrogel

The swelling ratio (SR) is a very crucial parameter for evaluating hydrogels. The swelling measurements are carried out by the immersion of 0.1 g of each hydrogel with different polymer ratios and crosslinking ratios in distilled water. The swollen hydrogel was weighed after 1 and 24 h. The calculation of the SR value was carried out as follows:
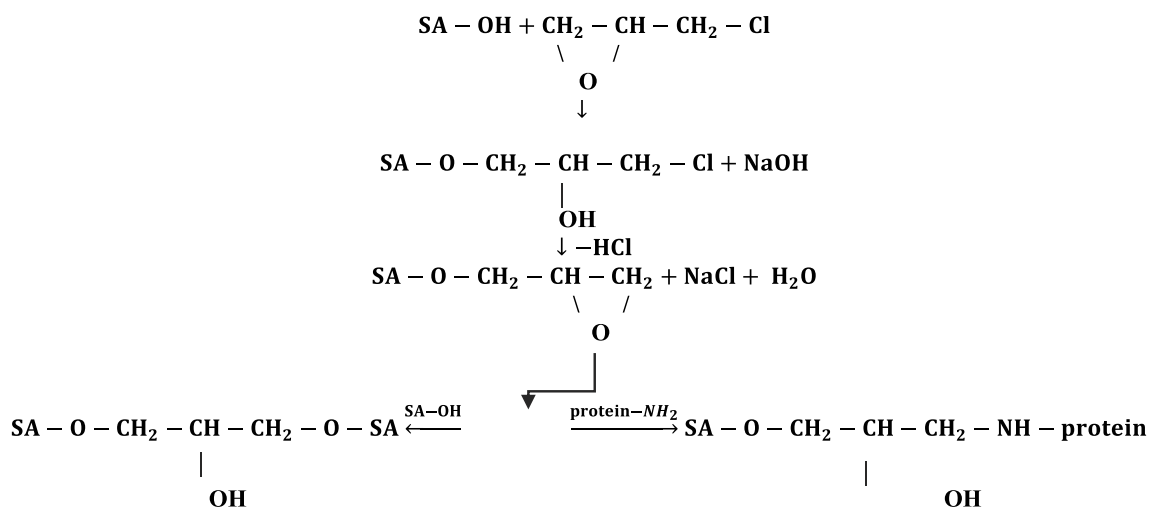
$$SR = \frac{W_s - W_d}{W_d} \tag{1}$$

where W_d and W_s are defined as the weights of the hydrogel before and after the swelling, correspondingly.

The surface morphology of the optimum and swollen SA/FG and SA/FGPEG hydrogels was defined by (Jeol (JSM—IT200), Japan) scanning electron microscopy. The 1-h swollen hydrogels were initially inserted for freeze-drying at −42 °C for 3 days to get rid of all absorbed water. Then, the samples were coated with gold for scanning.
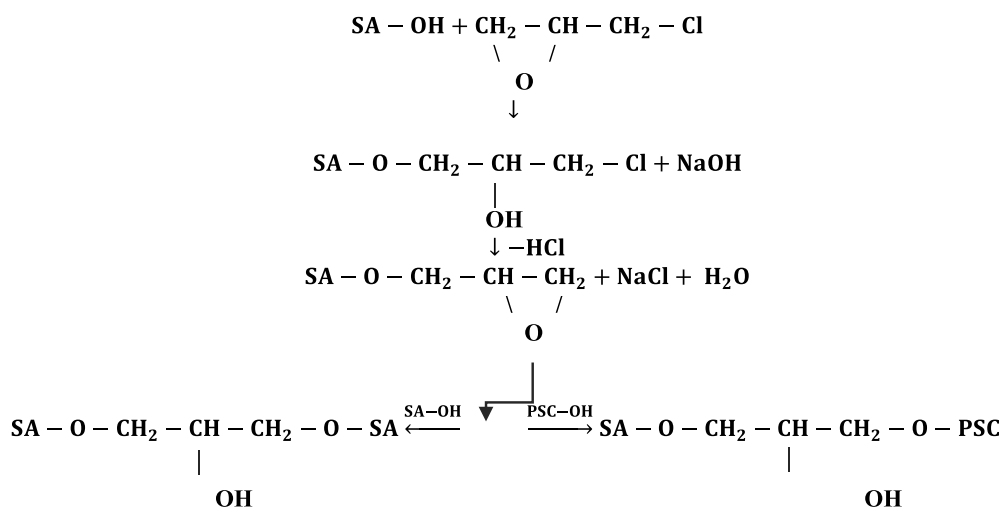
The compressive strength of SA/FG and SA/FG/PEG optimum and swollen hydrogels was measured at different distances using MultiTest-5xt, USA. The samples were

Table 2 All chemicals used in the experiments, their purity, and suppliers

Chemical	Purity (%)	Supplier
Sodium alginate (SA)	96.6	Oxford Lab Fine Chem LLP (India)
Polyethylene glycol (PEG)	99	Sigma-Aldrich (USA)
Sodium hydroxide	–	Alahram company (Egypt)
Epichlorohydrin (ECH)	92.5	LOBA CHEME (India)
Acetone	99	ADWIC (Egypt)

$$SA - OH + CH_2 - CH - CH_2 - Cl$$
$$\backslash \quad /$$
$$O$$
$$\downarrow$$

$$SA - O - CH_2 - CH - CH_2 - Cl + NaOH$$
$$|$$
$$OH$$
$$\downarrow\ -HCl$$
$$SA - O - CH_2 - CH - CH_2 + NaCl + H_2O$$
$$\backslash \quad /$$
$$O$$

$$SA - O - CH_2 - CH - CH_2 - O - SA \xleftarrow{SA-OH} \qquad \xrightarrow{protein-NH_2} SA - O - CH_2 - CH - CH_2 - NH - protein$$
$$| \qquad\qquad\qquad\qquad\qquad\qquad\qquad\qquad\qquad\qquad |$$
$$OH \qquad\qquad\qquad\qquad\qquad\qquad\qquad\qquad\qquad OH$$

(a) Crosslinking reaction between protein and sodium alginate

$$SA - OH + CH_2 - CH - CH_2 - Cl$$
$$\backslash \quad /$$
$$O$$
$$\downarrow$$

$$SA - O - CH_2 - CH - CH_2 - Cl + NaOH$$
$$|$$
$$OH$$
$$\downarrow\ -HCl$$
$$SA - O - CH_2 - CH - CH_2 + NaCl + H_2O$$
$$\backslash \quad /$$
$$O$$

$$SA - O - CH_2 - CH - CH_2 - O - SA \xleftarrow{SA-OH} \qquad \xrightarrow{PSC-OH} SA - O - CH_2 - CH - CH_2 - O - PSC$$
$$| \qquad\qquad\qquad\qquad\qquad\qquad\qquad\qquad\qquad\qquad |$$
$$OH \qquad\qquad\qquad\qquad\qquad\qquad\qquad\qquad\qquad OH$$

(b) Crosslinking reaction between polysaccharides and sodium alginate

Fig. 1 Scheme of all possible crosslinking reactions between FG and SA

prepared in a cylinder shape. Samples were immersed in distilled water for an hour. The surface area of the swollen cylinder was 4.9 cm^2, and its length was 2 cm. The swollen samples were inserted into the device for the compression test measurements at 25 °C.

An X-ray powder diffractometer -XRD-D2 phaser (BRUKER, Germany) was applied to determine the XRD profiles of PEG, SA, and the optimized SA/FG/PEG hydrogel powders. The range of 2θ for all samples was from 10° to 100°.

The chemical composition of ECH liquid, extracted FG solution, SA, PEG, and the optimized SA/FG/PEG powder was confirmed by Fourier transform infrared spectroscopy (Bruker Tensor 37, Germany).

FO process

The FO batch unit that was applied for all FO experiments is clearly illustrated in Fig. 2. Prior to each run, the membrane was immersed in distilled water for 1 h for conditioning. At the beginning, the membrane's upper side was completely surfed by a very fine layer of dry powder hydrogel of defined average particle sizes. Then, the membrane was soaked in a beaker that contained the FS. The FS conductivity was measured by (DiST4, HI98304, Romani), and the weight of the hydrogel was recorded prior to and after the run. FS concentration and temperature and the average particle size of the hydrogel were the major parameters that were investigated in this FO process. The membrane's effective area was
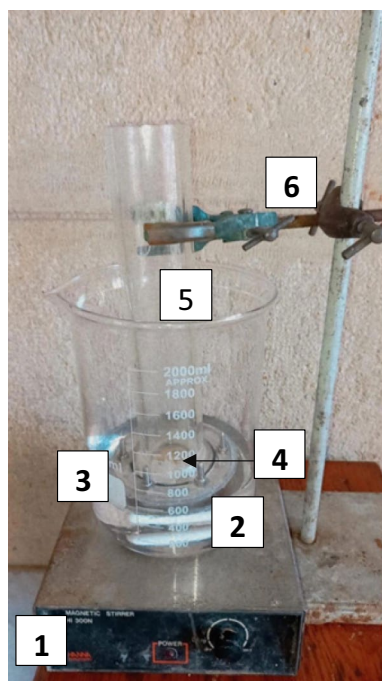
Fig. 2 Batch FO set up 1–magnetic stirring device, 2–magnetic stirring rod, 3–beaker, 4–hydrogel covers the top side of the membrane, 5–FO cell, and 6–holder

12.56 cm^2. The powder area density for all runs is 0.04 g/cm^2. The achieved water flux by this hydrogel was calculated as follows:

$$J_w = \frac{W_s - W_d}{\rho_w A t} \tag{2}$$

where J_w is the achieved water flux in each run; W_d and W_s are the masses of the hydrogel prior and after the FO run, respectively; ρ_w is the water density; A is the membrane surface area; and t is the time of each run.

Results and discussions

Hydrogel's characterizations

Swelling capacity

The osmotic pressure that originated from the dissociation of the ionic groups and the solvation force formed by the hydrogen bonds between the hydrogel network and water molecules is the major driving force for swelling. It is strongly affected by the polymer content and the degree of crosslinking (Bardhan et al. 2022).

Figure 3 illustrates how the PEG addition influences the swelling response of the hydrogel in 1 h at a constant FG/
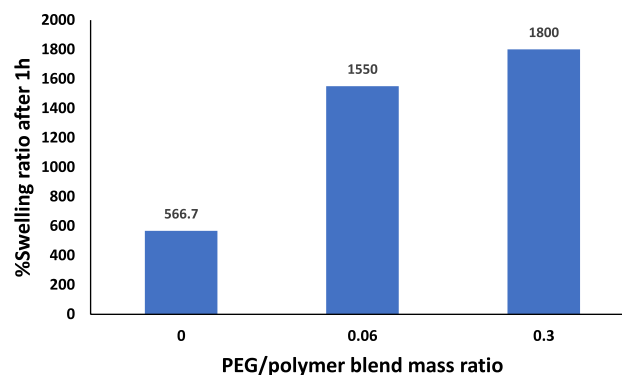
Fig. 3 Effect of PEG/polymer blend mass ratio on SR (%) (at 12% FG and 0.95 ECH/polymer blend mass ratio)

total polymer blend of 12% and ECH/total polymer blend of 0.95 mass ratio. It is well noted that the increase in PEG amount upgrades the hydrogel's response to absorb water. By upgrading the PEG mass ratio from zero to 0.3, the swelling ratio (%) nearly tripled from 566.7 to 1800 in 1 h. This can be explained by two main motives: Firstly, the design of semi-interpenetrating network hydrogel promotes the hydrogel's response to water absorption by enhancing water channeling within the crosslinked network (Ullah et al. 2015). Secondly, the hydrophilicity of PEG is due to the presence of an –O– group within its backbone, in addition to the existence of –OH terminal groups. These groups are able to create hydrogen bondings with water molecules, which consequently enhance water absorption (Mansur et al. 2004). The current trend and the earlier analysis are in agreement (Zhang et al. 2020). It is well clear that the mass ratio of 0.3 PEG/polymer blend is the best ratio.

The effect of FG (%) in the polymer blend on the swelling capacity was studied in two different time intervals of 1 and 24 h at the optimum PEG/polymer mass ratio of 0.3 and the constant ECH/total polymer mass ratio of 0.95. When the swelling behavior of the hydrogel with 12% FG was compared to that of the hydrogel with 0% FG, the consequence was that the addition of FG to the polymer blend increased swelling (%) in 1 h from 537.5 to 1800 and in 24 h from 3035.25 to 5300. The higher hydrophilicity of the extracted FG is what explains these observations (Łopusiewicz et al. 2022). Thus, the addition of the extracted, soluble FG portion to the polymer blend enhances water absorption. By increasing the FG (%) in the polymer blend from 12 to 100%, the swollen hydrogel became very soft and crumbled due to water pressure, so it was difficult to collect the very fine disintegrated parts. Consequently, the real weight of the swollen hydrogel and, hence, the swelling capacity cannot be correctly calculated. Moreover, the soft, swollen hydrogel loses its elasticity, which is considered a very critical mechanical property of the hydrogel (Okay 2009). From

these results, we can conclude that the best FG mass content in the crosslinker polymer blend was 12%.

Figure 4 signifies the impact of crosslinking dosage on SR (%) after 1 h and 24 h, at the constant mass ratio PEG/polymer blend of 0.3 and 12% FG in the crosslinked polymer blend. It is obviously noticeable that as the crosslinker dosage increases, the swelling ratio (%) reduces. As the dose of crosslinker rises, the polymer chains will be crosslinked more, and the polymer network will be more compact. Thus, the penetration of water molecules within the polymer network becomes harder, which leads to lower SR (Cui et al. 2018). From the studied values, the optimal ECH/polymer blend mass ratio was 0.95.

In summary, the best optimized hydrogel was that with 12% FG, a 0.95 ECH/polymer blend mass ratio, and a PEG/polymer blend mass ratio of 0.3.

SEM

The porosity of hydrogels influences their water absorption. As a result, hydrogel microstructure morphology is a significant property (Nakka and Mungray 2016). Figure 5

shows two images of the surface morphology of the neat SA/FG and the optimum SA/FG/PEG swollen hydrogel. After swelling, the hydrogel was freeze-dried for observation of pores that were previously filled with water molecules (Tu et al. 2017). The average pore size of the swollen neat SA/FG and SA/FG/PEG hydrogels was 46.84 μm and 58.84 μm, respectively. It is remarkable that the presence of PEG in the hydrogel enhances the pore structure of the hydrogel. This is because of the formation of an open channel system that is a result of the connection of spherical pores within the hydrogel and acts as a capillary system. This consequently leads to rapid water uptake and dewatering. All results are agreed with the earlier study (Zhang et al. 2020).

Compression strength test

The compression strength measurements of the neat SA/FG and the optimal SA/FG/PEG swollen hydrogels were investigated to represent how the PEG addition impacts the mechanical strength of the swollen hydrogel. Typically, a compression strength test is recommended to identify the mechanical stability of the hydrogel through its regeneration

Fig. 4 Influence of ECH/polymer blend mass ratio on SR (%) in two different time intervals (at 12% FG and 0.3 PEG/crosslinked polymer blend mass ratio)
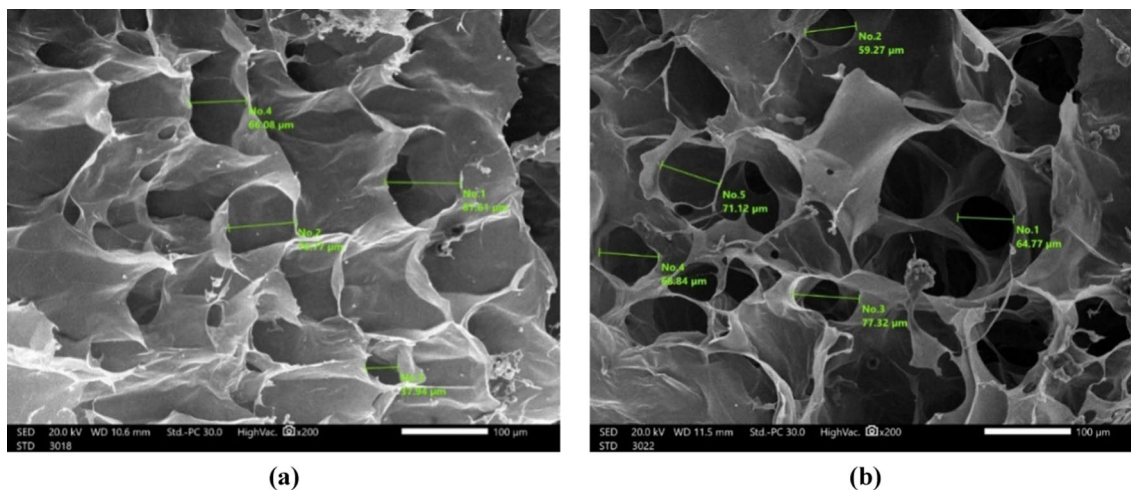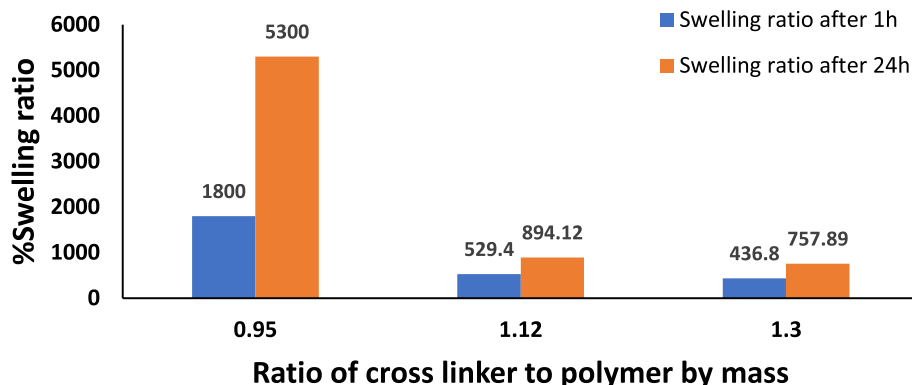
Fig. 5 Surface morphology (at 200×magnification) for **a** neat swollen SA/FG hydrogel and **b** optimum swollen SA/FG/PEG hydrogel
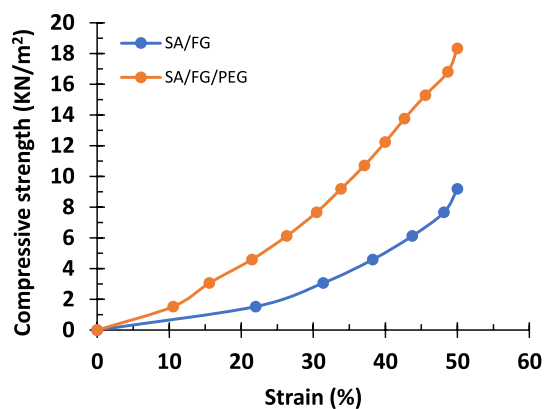
Fig. 6 Compressive strength versus strain of the neat SA/FG and the optimum SA/FG/[PEG swollen hydrogels

Table 4 Representation of the compression strength at 50% strain and the modulus of elasticity of the swollen SA/FG and SA/FG/PEG hydrogels

Hydrogel	Compressive strength $(3\ KN/m^2)$	Modulus of elasticity $(3\ KN/m^2)$
SA/FG	9.17	8.8
SA/FG/PEG	18.3	20.5

by squeezing. Actually, the detailed regeneration process could be studied in a separate, postponed study. Figure 6 shows the results of the compression strength tests of SA/FG and SA/FG/PEG hydrogels. The results revealed that the swollen neat hydrogel can withstand a compressive strength of 9.17 KN/m^2 while the optimum swollen hydrogel containing PEG can tolerate a compressive strength of 18.3 KN/m^2 when both hydrogels were compressed to their half-length without any deterioration of the hydrogel.

These results show the positive effect of PEG addition on the mechanical strength of the hydrogel. This is because of four main reasons: (a) Generally, the design of semi-interpenetrating network or even interpenetrating networks provides promoted mechanical properties, when compared to the basic copolymer hydrogels (Mandal et al. 2009; Ullah et al. 2015), (b) the incorporation of a synthetic polymer (PEG) to the crosslinked green blend of SA and FG surely enhances the compression strength as it is well-known that the mechanical strength of the synthetic polymers is extremely higher than that of natural polymers (Khansari et al. 2017; Sampath et al. 2017), (c) PEG is widely recommended in various applications as it is characterized with its outstanding mechanical strength (Chan et al. 2012; Amoozgar et al. 2012), and (d) with increased PEG dosage, the effects of physical entanglement and hydrogen bonding were more pronounced, acting as physical crosslinking points between PEG, SA, and FG. This subsequently supports the required compression strength (Zhu et al. 2015).

Table 4 shows the compressive strengths of SA/FG and SA/FG/PEG swollen hydrogels at a strain of 50% and their modulus of elasticity. The capacity of a material to resume its original shape and dimensions following the removal of a load is known as its elastic property. Because a hydrogel made of a polymer network exploits the idea of initially established rubber elasticity, it is therefore a very important mechanical attribute to study (Anseth et al. 1996). From

Table 2, the modulus of elasticity of the swollen SA/FG/PEG hydrogel was more than twice that of the swollen SA/FG hydrogel. This proves the positive effect of PEG incorporation on the elasticity of the hydrogel. Indeed, the present results are agreed with earlier researches that have investigated the impact of PEG incorporation on the mechanical performance of the hydrogel. Chan et al. synthesized a robust and semi-interpenetrating hydrogel from polyethylene glycol and collagen and studied the impact of PEG dosage on the mechanical characteristics of the hydrogel. They found that the increase in PEG content upgraded the compressive strength of the hydrogel at 50% strain and its modulus of elasticity (Chan et al. 2012).

FTIR

Figure 7 shows the IR spectra of ECH, SA, FG extract, PEG, and the optimum SA/FG/PEG hydrogel. For ECH, the C–C symmetric deformation of the epoxide groups is characterized by the vibrations at 925 and 962 cm^{-1} (Motillon et al. 2013). Regarding the IR spectrum of PEG, the broad peak at 3432.36 cm^{-1} corresponds to the terminal hydroxyl group. The peaks at 2883.56 cm^{-1} and 1105.93 cm^{-1} correspond to CH– and C–O stretching, respectively (Chieng et al. 2013).

In terms of the IR spectrum of SA, the OH stretching is characterized by broad peak of 3400.5 cm^{-1}, whereas the C–H stretching vibrations was defined by the peaks around 2928.82 cm^{-1}. The symmetrical and asymmetrical stretching of the carboxylate salt group are characterized by the peaks at 1416 and 1601 cm^{-1}, correspondingly. Moreover, the stretching of the C–O–C group is defined by the peak at 1023.45 cm^{-1} (Merakchi 2019).

The IR spectrum of FG shows a strong peak at 3462.4, which can be attributed to OH or N–H stretching, where both appear in the same region (Socrates 2004). The peak at 1639.89 cm^{-1} is due to the C=O asymmetrical stretching vibration of the carboxylate salt group. The crystallinity of gum is symbolized by the area between 700 and 500 cm^{-1}. So, the crystalline nature of biopolymers is characterized by the peak at 684.7 cm^{-1} (Rashid et al. 2019).

In the FTIR spectrum of the present SA/FG/PEG hydrogel, the major peak at 3436.12 cm^{-1} is because of the N–H or OH stretching vibration. It is well obvious that the

Fig. 7 FTIR spectrum of ECH, PEG, SA, FG extract, and optimum dry SA/FG/PEG hydrogel
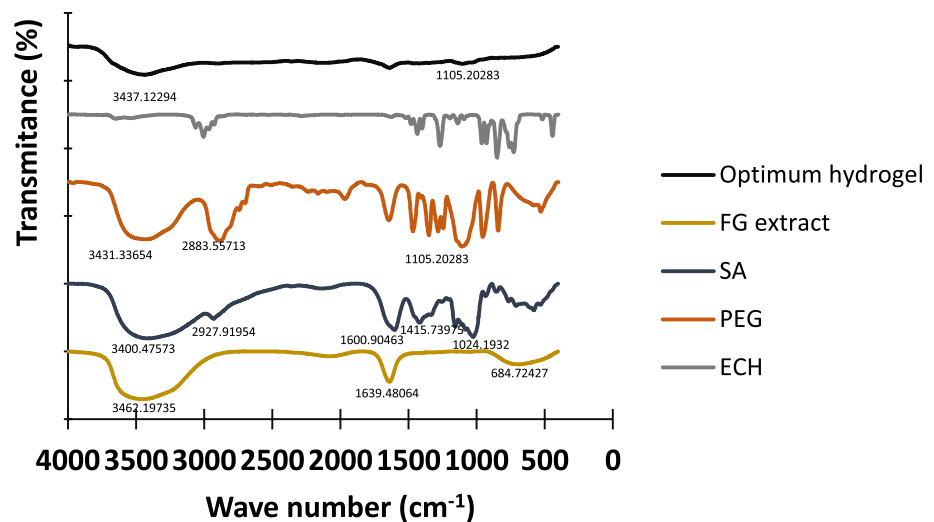
intensity of such a peak decreased compared to the same peaks associated with SA and FG, respectively. The decline of the peak intensity can be attributed to the fact that some of the OH and N–H groups are incorporated in crosslinking reactions with other polymeric chains of either SA chains or FG chains according to the scheme as shown in Fig. 1. The peak of 1104.43 cm^{-1} confirms the presence of PEG as a semi-interpenetrating chain within the hydrogel. The two peaks at 1640 and 1421.33 cm^{-1} are due to C=O asymmetrical and symmetrical stretching vibrations, respectively, of the carboxylate salt group, which are present in SA and FG. The peak at 1023.45 cm^{-1}, which exists in the SA spectrum, is shifted to 1104.43 cm^{-1} in the hydrogel spectrum. The peaks at 962 and 925 cm^{-1} that symbolize the epoxide group of ECH have vanished. This confirms that the epoxide ring opened owing to the crosslinking reaction. All of these results confirm the crosslinking reaction between SA and FG using ECH.

XRD

Figure 8 demonstrates the XRD spectra of SA, PEG, and the present optimal SA/FG/PEG hydrogel consequently. The XRD spectrum of SA exhibits weak peaks and broad diffraction at 15° and 22.1°. This consequently confirms the amorphous structure of SA (Zheng et al. 2016). Regarding the XRD spectrum of PEG, there are two major peaks at 19.318 and 23.32°, while there are other minor peaks at 26.40°, 36.28°, 39.74°, and 45.22°. These observations are consistent with earlier studies (Jayaramudu et al. 2016).

The XRD pattern of the present hydrogel shows that the weak peaks attributed to SA have vanished. This is considered a confirmation of the crosslinking reaction between SA and FG and consequently causes the amorphous structure of the hydrogel. The strong peaks at $2\Theta = 19.31°$ and 23.32° corresponding to PEG are still obvious in the XRD

of the hydrogel, which indicates that PEG is present as a semi-interpenetrating linear polymer and does not interact chemically with SA and FG.

FO batch experiments

In the preliminary experiments by applying distilled water as FS, when FO mode (support layer facing draw agent) was applied in the FO batch setup, it was found that the support layer was clogged with the hydrogel's particles, which definitely reduced the driving force and hence the water flux. Accordingly, all the following FO runs were carried out by applying PRO mode (active layer facing draw agent). Actually, PRO mode is more recommended than FO mode in the desalination of synthetic saline water and brackish water owing to the enhanced water flux achieved (Zhao et al. 2011).
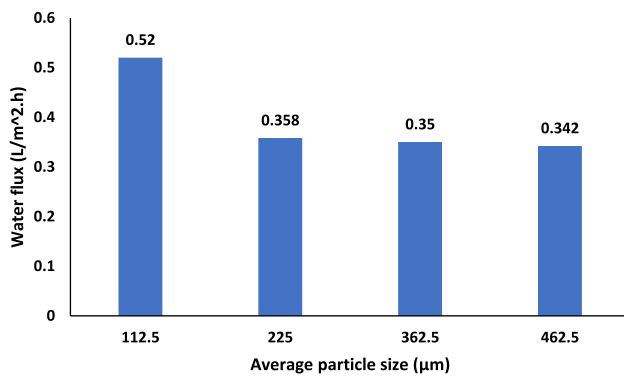
Impact of hydrogel's particle size

One of the most essential factors affecting the behavior of the hydrogel as a draw agent in the FO process is its average particle size. Figure 9 shows how the average particle size of the hydrogel influences the achieved water flux. It is strongly noticed that by reducing the average particle size of the hydrogel, water flux rises. This may be attributed to two main facts: (i) The smaller size of the hydrogel particle can lead to a higher contact area between the membrane and the hydrogel. Thus, the hydrogel will be able to absorb a larger amount of water (Li et al. 2013). (ii) According to gel dynamics theory, the hydrogel swelling rate is inversely proportional to the square of hydrogel size and proportional to the diffusion coefficient of the hydrogel. Thus, water flux will be increased at smaller hydrogel particle sizes (Wang et al. 2020).

Fig. 8 XRD spectrum of **a** SA, **b** PEG, and **c** optimal SA/FG/PEG hydrogel


(a)

(b)

(c)
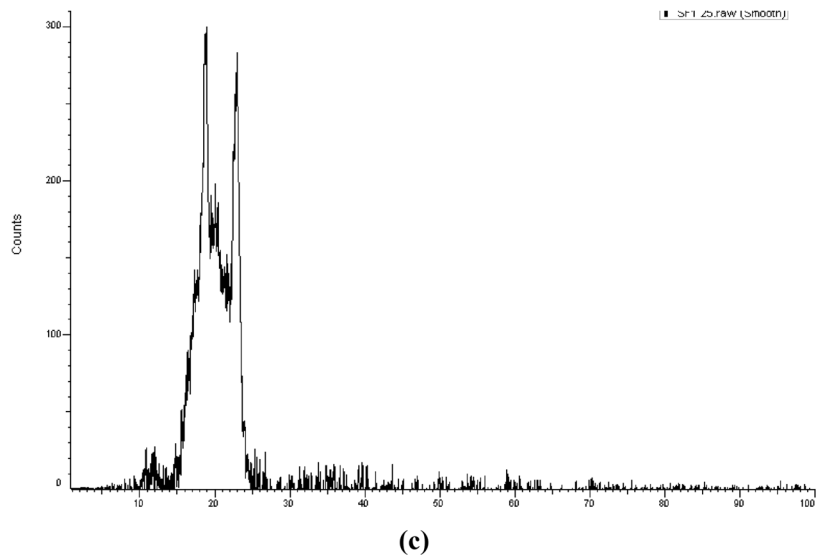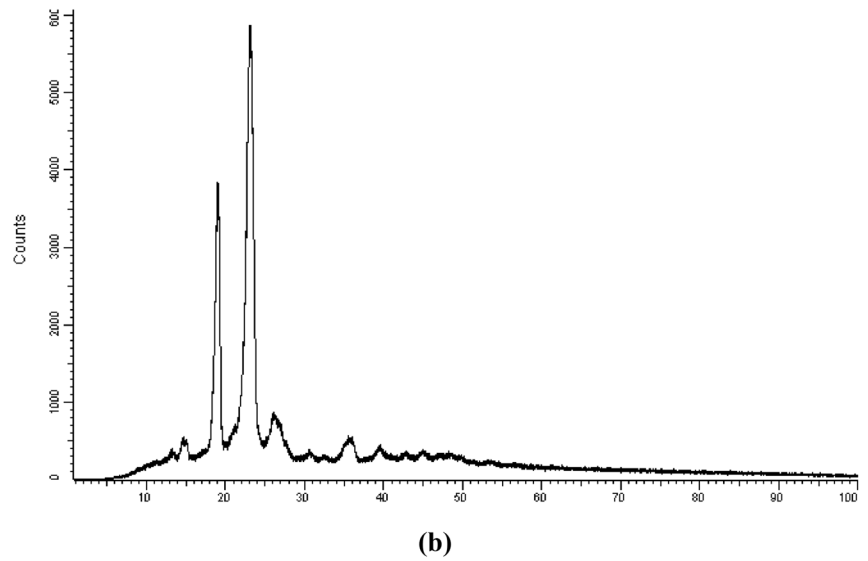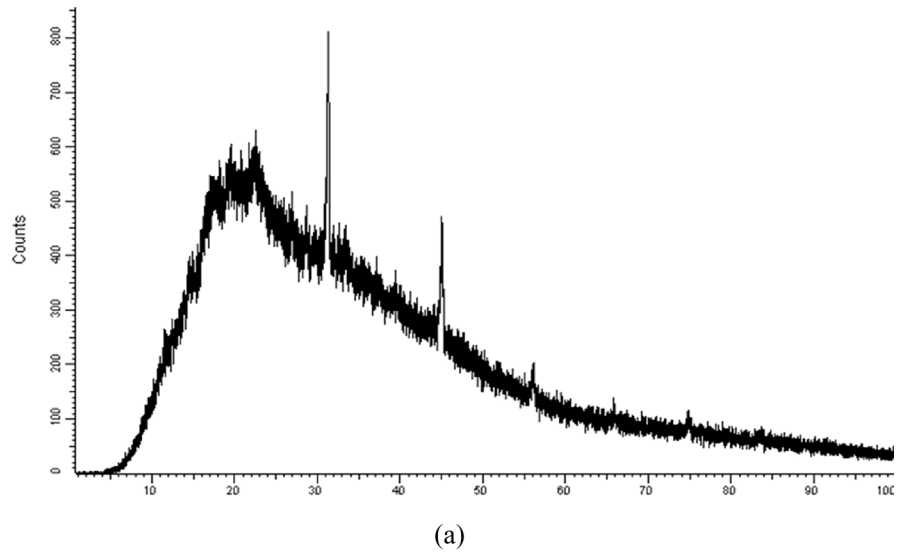
Fig. 9 Effect of average hydrogel's particle size on water flux (at 30 °C and distilled water as feed solution)

Impact of FS temperature

Figure 10 displays how the FO water flux affected by FS temperature. It is clearly observed that rising FS temperatures encourage water flux. By raising the FS temperature from 23 to 35 °C, the water flux is nearly tripled. This is because of the reduction of FS viscosity, which consequently upgrades the diffusion coefficient, according to the Stokes–Einstein equation (Erin 2020; Denton 2004). Subsequently, the diffusion of FS from the FS side to the DS side will be enhanced. In addition, as studied in previous articles, the increase in the FS temperature within the range of 20–40 °C has a negligible impact on the CTA membrane structural parameter (S). So, the membrane polymer structure will be conserved without any deterioration during processing at FS temperatures up to 35 °C. Moreover, the water permeability (A) parameter will be enhanced by raising the FS temperature to 35 °C (Xie et al. 2013).
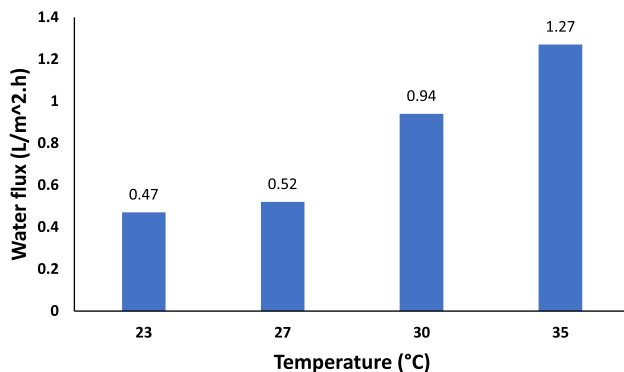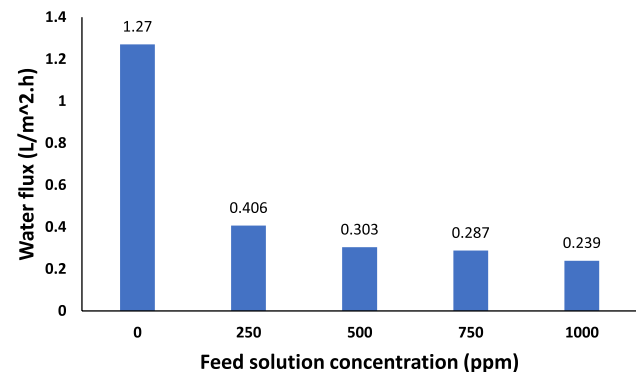
Influence FS concentration

Figure 11 represents the impact of FS concentration on the water flux. It is obvious that the increase in the FS concentration has a negative effect on the produced water flux. This is because the increase in the ionic strength of FS leads to lower osmotic pressure, and hence the water flux diminishes. The current trend is agreed with earlier researches (Zhang et al. 2020; Li et al. 2011).

From all the above FO experiments, we can say that the best performance of our FO batch setup was at a water flux of 1.27 LMH when distilled water was used as FS, the hydrogel with an average particle size of 112.5 μm was applied as a draw agent, and the FS temperature was 35 °C.

When this work was compared with previous studies, we found that our results were very comparable to the results published by Cai et al. (2013) and Zeng et al. (2019). Cai et al. prepared a semi-IPN thermoresponsive hydrogel by polymerizing N-isopropylacrylamide (NIPAm) in the existence of polysodium acrylate (PSA) or polyvinyl alcohol. Zeng et al. prepared two different designs of the same hydrogel to apply them as draw agents in FO desalination: a single-layer hydrogel prepared by the copolymerization of NIPAm and SA and a multi-layer hydrogel composed of a drawing layer rich in SA and a releasing layer rich in NIPAm. The best-performing hydrogel in each design was that with a polymer ratio of 1:1 in the single layer or the drawing layer. In addition, our present work is completely superior to our previous work, which prepared a bioartificial hydrogel from a blend of SA and PVA (Saad et al. 2023). This can be explained by the following reasons: (a) the semi-IPN design of our present work, which improves the hydrogel's response; and (b) the replacement of PVA with FG, which is richer with hydrophilic groups and consequently enhances water flux. All water fluxes achieved in an hour by the mentioned previous works and our present work are described briefly in Table 5.

Fig. 10 Influence of FS temperature on water flux (at average hydrogel's particle size of 112.5 μm and distilled water as FS)

Fig. 11 Impact of FS concentration on water flux (at FS temperature of 35 °C and average hydrogel's particle size was 112.5 μm)

Table 5 Representation of the FO water fluxes achieved by the previous studies and the present work

Hydrogel	Temperature	Feed solution	Water flux (LMH)
NIPAm-co-SA (single layer	25 °C	2000 ppm NaCl solution	0.295
NIPAm-co-SA (multi-layer)	25 °C	2000 ppm NaCl solution	0.292
NIPAm/PSA	25 °C	2000 ppm NaCl solution	0.18
NIPAm/PVA	25 °C	2000 ppm NaCl solution	0.12
SA/PVA	40 °C	Distilled water	0.845 (1 h)
		250 ppm NaCl solution	0.399 (1 h)
		500 ppm NaCl solution	0.359 (1 h)
		750 ppm NaCl solution	0.279 (1 h)
		1000 ppm NaCl solution	0.129 (1 h)
SA/FG/PEG (present work)	35 °C	Distilled water	1.27
		250 ppm NaCl solution	0.406
		500 ppm NaCl solution	0.303
		750 ppm NaCl solution	0.287
		1000 ppm NaCl solution	0.239

Moreover, real brackish water from two distinct wells with TDS of 1160.8 and 1633.16 ppm was applied as FS at 35 °C with an average hydrogel's particle size of 112.5 μm. The results revealed that the achieved water fluxes were 0.254 and 0.27 LMH, respectively.

Reverse solute flux

The solute diffusion from the draw solution side to the FS side due to the concentration gradient across the membrane is defined as the reverse solute flux (RSF). This phenomenon negatively affects on the driving force in the FO process (Xu et al. 2022a). In this current study, a hydrogel is applied as a draw agent, which is a solid material with a high water absorption capacity, so there is no concentration gradient, and hence, reverse solute flux is negligible in all FO experiments (Zhang et al. 2015). The insignificant RSF was confirmed by conductivity measurements of distilled water, which was applied as FS in FO experiments. Typically, conductivity measurements of distilled water provide the most accurate indication of RSF as it achieves the highest driving force when compared to other feed solutions with higher concentrations. The conductivity of the distilled water before and after the FO run was recorded at 0.01 μS/cm, which means that there was no RSF accomplished. These results are comparable to those of previous studies mentioned in Table 1.

Conclusions

A novel green hydrogel was prepared from a polymer blend of sodium alginate (SA) and flaxseed gum (FG) extracted from flaxseed and used epichlorohydrin (ECH) as a crosslinker and polyethylene glycol (PEG) as a semi-interpenetrating network polymer. The obtained hydrogel was characterized by swelling ratio measurements, FTIR, XRD, SEM, and compression strength tests. The performance of this hydrogel as a draw agent in a batch FO unit was studied by varying the average hydrogel's particle size and FS temperature and concentration parameters. The results can be summarized as follows:

- The increase in PEG/total polymer blend mass ratio and %FG in the polymer blend enhances swelling ratio (%), while rising ECH/total polymer blend downgrades it.
- PRO mode is more preferred than FO mode.
- FS temperature has a positive impact on the water flux, while the average hydrogel particle size and FS concentration have a reverse effect on it.
- The RSF in all FO experiments is negligible.

Declarations

Conflict of interest There are no conflicts of interest associated to this manuscript.

References

Allamraju KV (2021) Green Hydrogels. Green Compos 225–249

Altaee A, Zaragoza G, van Tonningen HR (2014) Comparison between forward osmosis-reverse osmosis and reverse osmosis processes for seawater desalination. Desalination 336:50–57

Amoozgar Z, Rickett T, Park J, Tuchek C, Shi R, Yeo Y (2012) Semi-interpenetrating network of polyethylene glycol and photo-crosslinkable chitosan as an in-situ-forming nerve adhesive. Acta Biomater 8:1849–1858

Ankoliya D, Mehta B, Raval H (2019) Advances in surface modification techniques of reverse osmosis membrane over the years. Sep Sci Technol 54:293–310

Anseth KS, Bowman CN, Brannon-Peppas L (1996) Mechanical properties of hydrogels and their experimental determination. Biomaterials 17:1647–1657

Baker B, Aldridge C, Omer A (2016) Water: availability and use. Mississippi State University Extension, 2016, p 3011

Bardhan A, Subbiah S, Mohanty K, Ibrar I, Altaee A (2022) Feasibility of poly (vinyl alcohol)/poly (diallyldimethylammonium chloride) polymeric network hydrogel as draw solute for forward osmosis process. Membranes 12:1097

Bo J (1992) Study on PVA hydrogel crosslinked by epichlorohydrin. J Appl Polym Sci 46:783–786

Buhus G, Peptu C, Popa M, Desbrieres J (2009) Controlled release of water soluble antibiotics by carboxymethylcellulose-and gelatin-based hydrogels crosslinked with epichlorohydrin. Cellul Chem Technol 43:141

Cai Y, Shen W, Loo SL, Krantz WB, Wang R, Fane AG, Hu X (2013) Towards temperature driven forward osmosis desalination using semi-IPN hydrogels as reversible draw agents. Water Res 47:3773–3781

Chan BK, Wippich CC, Wu CJ, Sivasankar PM, Schmidt G (2012) Robust and semi-interpenetrating hydrogels from poly (ethylene glycol) and collagen for elastomeric tissue scaffolds. Macromol Biosci 12:1490–1501

Chatterjee S, Hui PC-l (2018) Stimuli-responsive hydrogels: an interdisciplinary overview. Hydrogels—Smart Materials for Biomedical Applications, pp 1–23

Chieng BW, Ibrahim NA, Wan Yunus WMZ, Hussein MZ (2013) Poly (lactic acid)/poly (ethylene glycol) polymer nanocomposites: effects of graphene nanoplatelets. Polymers 6:93–104

Cui H, Zhang H, Yu M, Yang F (2018) Performance evaluation of electric-responsive hydrogels as draw agent in forward osmosis desalination. Desalination 426:118–126

Denton EL (2004) Liquid viscosity and temperature (J1511). In: California state science fair

Ellis SN, Cunningham MF, Jessop PG (2021) A forward osmosis hydrogel draw agent that responds to both heat and CO_2. Desalination 510:115074

Erin E (2020) The relationship between diffusion coefficients and viscosity in organic-water matrices as proxies for secondary organic aerosols. In: Chemistry. B.Sc., The University of Western Ontario, 2015

Esposito L, Barbosa AI, Moniz T, Costa Lima S, Costa P, Celia C, Reis S (2020) Design and characterization of sodium alginate and poly (vinyl) alcohol hydrogels for enhanced skin delivery of quercetin. Pharmaceutics 12:1149

Hu Y, Shim YY, Reaney MJ (2020) Flaxseed gum solution functional properties. Foods 9:681

Jain H, Kumar A, Rajput VD, Minkina T, Verma AK, Wadhwa S, Dhupper R, Garg MC, Joshi H (2022a) Fabrication and characterization of high-performance forward-osmosis membrane by introducing manganese oxide incited graphene quantum dots. J Environ Manag 305:114335

Jain H, Kumar A, Verma AK, Wadhwa S, Rajput VD, Minkina T, Garg MC (2022b) Treatment of textile industry wastewater by using high-performance forward osmosis membrane tailored with alpha-manganese dioxide nanoparticles for fertigation. Environ Sci Pollut Res 29:80032–80043

Jayaramudu T, Raghavendra GM, Varaprasad K, Reddy GVS, Reddy AB, Sudhakar K, Sadiku ER (2016) Preparation and characterization of poly (ethylene glycol) stabilized nano silver particles by a mechanochemical assisted ball mill process. J Appl Polym Sci. https://doi.org/10.1002/app.43027

Ju H, McCloskey BD, Sagle AC, Kusuma VA, Freeman BD (2009) Preparation and characterization of crosslinked poly (ethylene glycol) diacrylate hydrogels as fouling-resistant membrane coating materials. J Membr Sci 330:180–188

Khansari MM, Sorokina LV, Mukherjee P, Mukhtar F, Shirdar MR, Shahidi M, Shokuhfar T (2017) Classification of hydrogels based on their source: a review and application in stem cell regulation. JOM 69:1340–1347

Li D, Zhang X, Yao J, Zeng Y, Simon GP, Wang H (2011) Composite polymer hydrogels as draw agents in forward osmosis and solar dewatering. Soft Matter 7:10048–10056

Li D, Zhang X, Simon GP, Wang H (2013) Forward osmosis desalination using polymer hydrogels as a draw agent: influence of draw agent, feed solution and membrane on process performance. Water Res 47:209–215

Liu J, Shim YY, Timothy JT, Wang Y, Reaney MJ (2018) Flaxseed gum a versatile natural hydrocolloid for food and non-food applications. Trends Food Sci Technol 75:146–157

Łopusiewicz Ł, Dmytrów I, Mituniewicz-Małek A, Kwiatkowski P, Kowalczyk E, Sienkiewicz M, Drozłowska E (2022) Natural gum from flaxseed by-product as a potential stabilizing and thickening agent for acid whey fermented beverages. Appl Sci 12:10281

Mandal BB, Kapoor S, Kundu SC (2009) Silk fibroin/polyacrylamide semi-interpenetrating network hydrogels for controlled drug release. Biomaterials 30:2826–2836

Mansur HS, Oréfice RL, Mansur AA (2004) Characterization of poly (vinyl alcohol)/poly (ethylene glycol) hydrogels and PVA-derived hybrids by small-angle X-ray scattering and FTIR spectroscopy. Polymer 45:7193–7202

Matricardi P, Di Meo C, Coviello T, Hennink WE, Alhaique F (2013) Interpenetrating polymer networks polysaccharide hydrogels for drug delivery and tissue engineering. Adv Drug Deliv Rev 65:1172–1187

Merakchi A (2019) Cross linking and modification of sodium alginate biopolymer for dye removal in aqueous solution. Polym Bull 76:3535–3554

Mohammadinejad R, Maleki H, Larrañeta E, Fajardo AR, Nik AB, Shavandi A, Sheikhi A, Ghorbanpour M, Farokhi M, Govindh P, Cabane E, Azizi S, Aref AR, Mozafari M, Mehrali M, Thomas S, Mano JF, Mishra YK, Thakur VK (2019) Status and future scope of plant-based green hydrogels in biomedical engineering. Appl Mater Today 16:213–246

Motillon C, Allal A, Visse A, Baldé A, Charrier F, Charrie B (2013) Bio-based thermoset resins for bonding and eco-friendly preservation in the wood industry. In: proceedings IRG annual meeting (ISSN 2000–8953)

Nakka R, Mungray AA (2016) Biodegradable and biocompatible temperature sensitive triblock copolymer hydrogels as draw agents for forward osmosis. Sep Purif Technol 168:83–92

Ohtani E (2021) Hydration and dehydration in Earth's interior. Annu Rev Earth Planet Sci 49:253–278

Okay O (2009) General properties of hydrogels. Hydrogel sensors and actuators. Springer, Berlin, Heidelberg, pp 1–14

Pan Z, Huang Y, Yang X, Liang Y, He J, Yu H (2022) Synthesis and characterization of sewage sludge ash-based temperature-sensitive hydrogel as an advanced class of forward osmosis desalination draw agent. Environ Eng Sci 39:896–905

Rashid F, Ahmed Z, Hussain S, Huang J-Y, Ahmad A (2019) *Linum usitatissimum* L. seeds: flax gum extraction, physicochemical and functional characterization. Carbohyd Polym 215:29–38

Saad M, Sadik E, Eldakiky B, Moustafa H, Fadl E, He Z, Elashtokhy EZ, Khlifa R, Zewail T (2023) Synthesis and characterization of an innovative poly vinyl alcohol/sodium alginate bioartificial hydrogel for forward-osmosis desalination

Sampath UTM, Ching YC, Chuah CH, Singh R, Lin P-C (2017) Preparation and characterization of nanocellulose reinforced semi-interpenetrating polymer network of chitosan hydrogel. Cellulose 24:2215–2228

Socrates G (2004) Infrared and Raman characteristic group frequencies: tables and charts. John Wiley & Sons

Suwaileh W, Pathak N, Shon H, Hilal N (2020) Forward osmosis membranes and processes: a comprehensive review of research trends and future outlook. Desalination 485:114455

Tu KL, Simon GP, Wang H (2017) Fast-responsive monolithic hydrogels as draw agent for forward osmosis membrane process. Sep Sci Technol 52:2583–2590

Ullah F, Othman MBH, Javed F, Ahmad Z, Akil HM (2015) Classification, processing and application of hydrogels: a review. Mater Sci Eng C 57:414–433

USAID (2009) Addressing water challenges in the developing world: a framework for action. 1.32

Wang J, Gao S, Tian J, Cui F, Shi W (2020) Recent developments and future challenges of hydrogels as draw solutes in forward osmosis process. Water 12:692

Wen H, Xu N, Soyekwo F, Dou P, Liu C (2023) Towards enhanced performance of fertilizer-drawn forward osmosis process coupled with sludge thickening using a thin-film nanocomposite membrane interlayered with Mxene scaffolded alginate hydrogel. J Membr Sci 685:121899

Xie M, Price WE, Nghiem LD, Elimelech M (2013) Effects of feed and draw solution temperature and transmembrane temperature difference on the rejection of trace organic contaminants by forward osmosis. J Membr Sci 438:57–64

Xu Y, Zhu Y, Chen Z, Zhu J, Chen G (2022a) A Comprehensive review on forward osmosis water treatment: recent advances and prospects of membranes and draw solutes. Int J Environ Res Public Health 19:8215

Xu Z, Wu K, Luo H, Wang Q, Zhang TC, Chen X, Rong H, Fang Q (2022b) Electro-responsive semi-IPN hydrogel with enhanced responsive property for forward osmosis desalination. J Appl Polym Sci 139:51650

Younos T, Tulou KE (2005) Overview of desalination techniques. J Contemp Water Res Educ 132:3–10

Zeng J, Cui S, Wang Q, Chen R (2019) Multi-layer temperature-responsive hydrogel for forward-osmosis desalination with high permeable flux and fast water release. Desalination 459:105–113

Zhang H, Li J, Cui H, Li H, Yang F (2015) Forward osmosis using electric-responsive polymer hydrogels as draw agents: influence of freezing–thawing cycles, voltage, feed solutions on process performance. Chem Eng J 259:814–819

Zhang K, Li F, Wu Y, Feng L, Zhang L (2020) Construction of ionic thermo-responsive PNIPAM/γ-PGA/PEG hydrogel as a draw agent for enhanced forward-osmosis desalination. Desalination 495:114667

Zhao S, Zou L, Mulcahy D (2011) Effects of membrane orientation on process performance in forward osmosis applications. J Membr Sci 382:308–315

Zhao S, Zou L, Tang CY, Mulcahy D (2012) Recent developments in forward osmosis: opportunities and challenges. J Membr Sci 396:1–21

Zheng H, Yang J, Han S (2016) The synthesis and characteristics of sodium alginate/graphene oxide composite films crosslinked with multivalent cations. J Appl Polym Sci 133

Zhu J (2010) Bioactive modification of poly (ethylene glycol) hydrogels for tissue engineering. Biomaterials 31:4639–4656

Zhu B, Ma D, Wang J, Zhang S (2015) Structure and properties of semi-interpenetrating network hydrogel based on starch. Carbohyd Polym 133:448–455